STRUCTURAL BIOLOGY COMMUNICATIONS

ISSN 2053-230X

Characterization of the *Pseudomonas aeruginosa* T6SS PldB immunity proteins PA5086, PA5087 and PA5088 explains a novel stockpiling mechanism

Haiying Wen,[a] Zhi Geng,[b] Zengqiang Gao,[b] Zhun She[b]* and Yuhui Dong[b,c]*

[a]School of Life Sciences, University of Science and Technology of China, Hefei, Anhui 230027, People's Republic of China, [b]Multidiscipline Research Center, Institute of High Energy Physics, Chinese Academy of Sciences, Beijing 100049, People's Republic of China, and [c]University of Chinese Academy of Sciences, People's Republic of China. *Correspondence e-mail: shezhun@ihep.ac.cn, dongyh@ihep.ac.cn

Received 10 February 2020
Accepted 22 April 2020

Edited by A. Nakagawa, Osaka University, Japan

Keywords: X-ray crystallography; T6SS immunity proteins; stockpiling mechanism; electrostatic potential surface; PA5086; *Pseudomonas aeruginosa*; type VI secretion system.

PDB reference: PA5086, 6lch

Supporting information: this article has supporting information at journals.iucr.org/f

The bacterial type VI secretion system (T6SS) secretes many toxic effectors to gain advantage in interbacterial competition and for eukaryotic host infection. The cognate immunity proteins of these effectors protect bacteria from their own effectors. PldB is a T6SS trans-kingdom effector in *Pseudomonas aeruginosa* that can infect both prokaryotic and eukaryotic cells. Three proteins, PA5086, PA5087 and PA5088, are employed to suppress the toxicity of PldB-family proteins. The structures of PA5087 and PA5088 have previously been reported, but the identification of further distinctions between these immunity proteins is needed. Here, the crystal structure of PA5086 is reported at 1.90 Å resolution. A structural comparison of the three PldB immunity proteins showed vast divergences in their electrostatic potential surfaces. This interesting phenomenon provides an explanation of the stockpiling mechanism of T6SS immunity proteins.

1. Introduction

As one of the leading opportunistic pathogens of humans, *Pseudomonas aeruginosa* possesses a powerful type VI secretion system (T6SS) that can secrete a large variety of effector–immunity (E–I) pairs that affect many areas of interspecies competition and host invasion (Russell *et al.*, 2011; Ho *et al.*, 2014; Hood *et al.*, 2010). Two phospholipase D (PLD) family proteins, PldA and PldB, which exhibit dual HKD*XX*-*XX*D (HKD) motifs, have been identified as trans-kingdom T6SS effectors that can affect both bacterial and human cells (Russell *et al.*, 2013; Jiang *et al.*, 2014).

Three consecutive genes immediately adjacent to the *pldB* gene encode three immunity proteins, PA5086, PA5087 and PA5088, that can suppress the toxicity of PldB. Our group have reported the crystal structures of PA5087 and PA5088, which both consist of several Sel1-like repeats [SLRs, named after the *Caenorhabditis elegans sel-1* gene products that form helix–turn–helix (α/α) motifs] that fold into super-ring forms (Grant & Greenwald, 1996; Das *et al.*, 1998; Yang *et al.*, 2016). We observed that PA5087 and PA5088 share great structural similarity but differ in their electrostatic potential surfaces (Yang *et al.*, 2016).

Here, we present the 1.90 Å resolution crystal structure of PA5086, which possesses the same overall structure as its immunity protein neighbors PA5087 and PA5088 but is quite different from them in electrostatic potential surface. Our

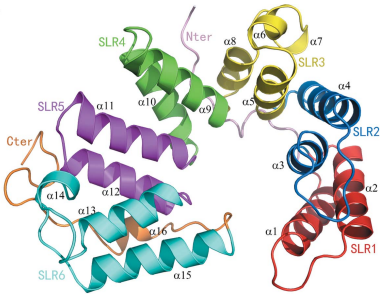

work completed the characterization of all three PldB immunity proteins and should aid future functional studies.

2. Materials and methods

2.1. Macromolecule production

The gene encoding PA5086 (without the N-terminal 21-residue signal peptide) was amplified from *P. aeruginosa* PAO1 genomic DNA. The PCR products were cloned into the pGEX-6T vector, which was a modification of the pGEX-6P-1 vector (GE Healthcare, Marlborough, Massachusetts, USA) by adding an N-terminal His_6 tag prior to the GST fusion tag and replacing the PreScission protease site with a Tobacco etch virus (TEV) protease cleavage site. The plasmid was then transformed into *Escherichia coli* BL21(DE3) cells. Large cultures were induced at an OD_{600} of 0.6 with a final concentration of 0.3 m*M* isopropyl β-D-1-thiogalactopyranoside (IPTG) and were left to express at 290 K for 18 h.

The cells containing PA5086 protein were pelleted, resuspended in buffer consisting of 20 m*M* Tris pH 8.0, 500 m*M* NaCl, 1 m*M* phenylmethylsulfonyl fluoride (PMSF) and disrupted using a high-pressure homogenizer. The lysate was centrifuged at 13 000*g* for 40 min. The supernatant containing the soluble protein was purified via affinity chromatography with nickel–nitrilotriacetic acid resin (Bio-Rad, Hercules, California, USA) and the His_6-GST tag was removed by overnight hydrolysis with TEV protease and reloading with 20 m*M* imidazole. The PA5086 protein was further purified by gel-filtration chromatography (Superdex 200, GE Healthcare, Marlborough, Massachusetts, USA) with buffer consisting of 20 m*M* Tris pH 8.0, 150 m*M* NaCl. The purified protein was

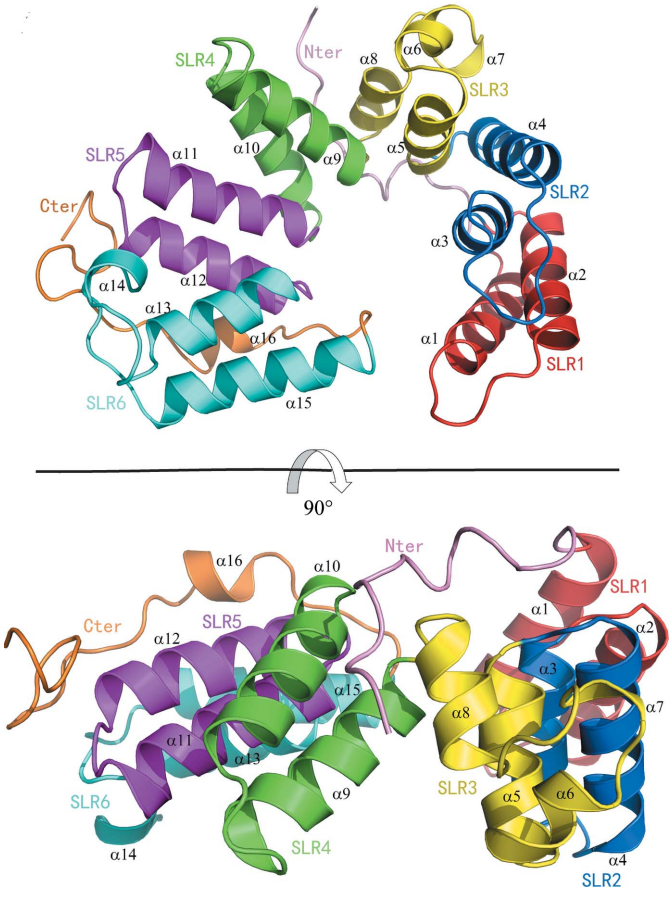

Figure 1
Top and side views of PA5086 in cartoon representation. The secondary-structure elements referred to in the text are labeled; SLR1, SLR2, SLR3, SLR4, SLR5 and SLR6 are colored red, blue, yellow, green, magenta and cyan, respectively.

Table 1
Macromolecule-production information.

Source organism	*P. aeruginosa*
DNA source	*P. aeruginosa* PAO1
Forward primer†	CGCGGATCCGCTGACAGCAAGCCTTTTGTC
Reverse primer‡	GGCCTCGAGTTACCGCTCCGGCTTCCAGTC
Cloning vector	pGEX-6T
Expression vector	pGEX-6T
Expression host	*E. coli* BL21(DE3)
Complete amino-acid sequence of the construct produced	GSADSKPFVCVNEKDHLPPLDPQADAWYRE AATLAKPDTLRPWPRIVGLYSKAAERGH WKAMHNLANLYRTGWPGGVEKDTQKALD LYQKMIDLDVPQGFYDMGAMIGNRAGVK NPATDGLTFLDKAASLGNPPALTELGKF YIYVAKKKDLGLAYTHCAASQGYAPASY ELGAYYKIVEHNFPKALVYYQVSVSQGG KSAAFFLSRVFGSETPPASAMWYAPDEK LREAYYSIYKKLEADPDLRFPNLIEDYP LPPHPTQGYDADRPDWKPER

† The BamHI site is underlined. ‡ The XhoI site is underlined.

Table 2
Crystallization.

Method	Sitting-drop vapor diffusion
Plate type	48-well
Temperature (K)	293
Protein concentration (mg ml^{-1})	19
Buffer composition of protein solution	20 m*M* Tris pH 8.0, 150 m*M* NaCl
Composition of reservoir solution	0.2 *M* sodium sulfate decahydrate, 20%(*w*/*v*) polyethylene glycol 3350
Volume and ratio of drop	1 µl protein solution:1 µl reservoir solution
Volume of reservoir (µl)	80

Table 3
Data collection and processing.

Values in parentheses are for the outer shell.

Diffraction source	Beamline 1W2B, BSRF
Wavelength (Å)	1.0000
Temperature (K)	100
Detector	SX165
Crystal-to-detector distance (mm)	124.3
Rotation range per image (°)	1
Total rotation range (°)	360
Exposure time per image (s)	10
Space group	*C*2
a, *b*, *c* (Å)	60.10, 63.20, 66.90
α, β, γ (°)	90, 105.00, 90
Mosaicity (°)	0.362
Resolution range (Å)	32.9–1.9 (1.95–1.90)
Total No. of reflections	138682 (9763)
No. of unique reflections	18481 (1291)
Completeness (%)	96.64 (94.13)
Multiplicity	7.5 (7.56)
$\langle I/\sigma(I)\rangle$	25.03 (8.91)
$R_{r.i.m.}$	0.05
Overall *B* factor from Wilson plot (Å^2)	10.8

collected and ultrafiltered to 19 mg ml^{-1}. Macromolecule-production information is summarized in Table 1.

2.2. Crystallization

Crystallization screening of PA5086 was carried out at 293 K using the sitting-drop vapor-diffusion technique. The best crystals of PA5086 were obtained within five weeks using a condition consisting of 0.2 *M* sodium sulfate decahydrate, 20%(*w*/*v*) polyethylene glycol 3350. Crystallization information is summarized in Table 2.

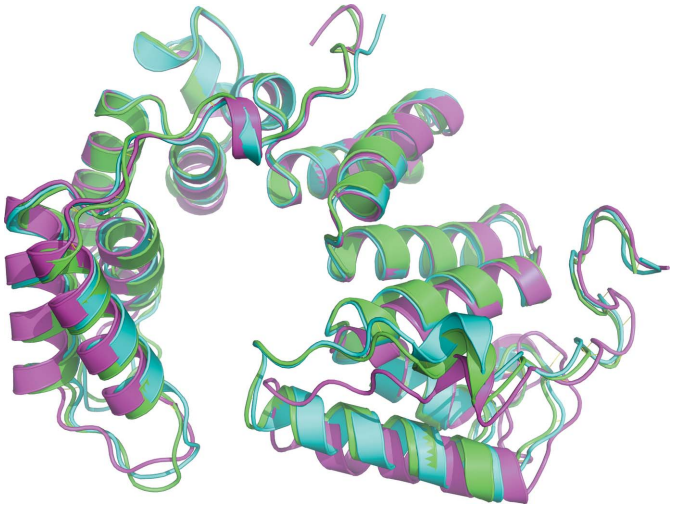

Figure 2
Structure superposition of PA5086 (green), PA5087 (cyan) and PA5088 (magenta).

Table 4
Structure refinement.

Values in parentheses are for the outer shell.

Resolution range (Å)	32.9–1.90 (1.95–1.90)
Completeness (%)	96.63
No. of reflections, working set	17529
No. of reflections, test set	952
Final R_{cryst}	0.229
Final R_{free}	0.266
Cruickshank DPI	0.222
No. of non-H atoms	
Protein	2085
Ligand	0
Water	256
Total	2341
R.m.s. deviations	
Bonds (Å)	0.005
Angles (°)	0.745
Average *B* factors (Å^2)	
Protein	13.1
Water	19.9
Overall	13.8
Ramachandran plot	
Favored regions (%)	95.8
Additionally allowed (%)	4.2
Outliers (%)	0

2.3. Data collection and processing

A data set was collected from a PA5086 crystal at 100 K at station 1W2B at Beijing Synchrotron Radiation Facility (BSRF). All data were initially integrated, scaled and merged using the *XDS* package (Kabsch, 2010) and were processed using the *CCP*4 suite (Winn *et al.*, 2011; Potterton *et al.*, 2018). Initial phases were acquired by molecular replacement using the structure of PA5087 (PDB entry 5jkp; Yang *et al.*, 2016) as

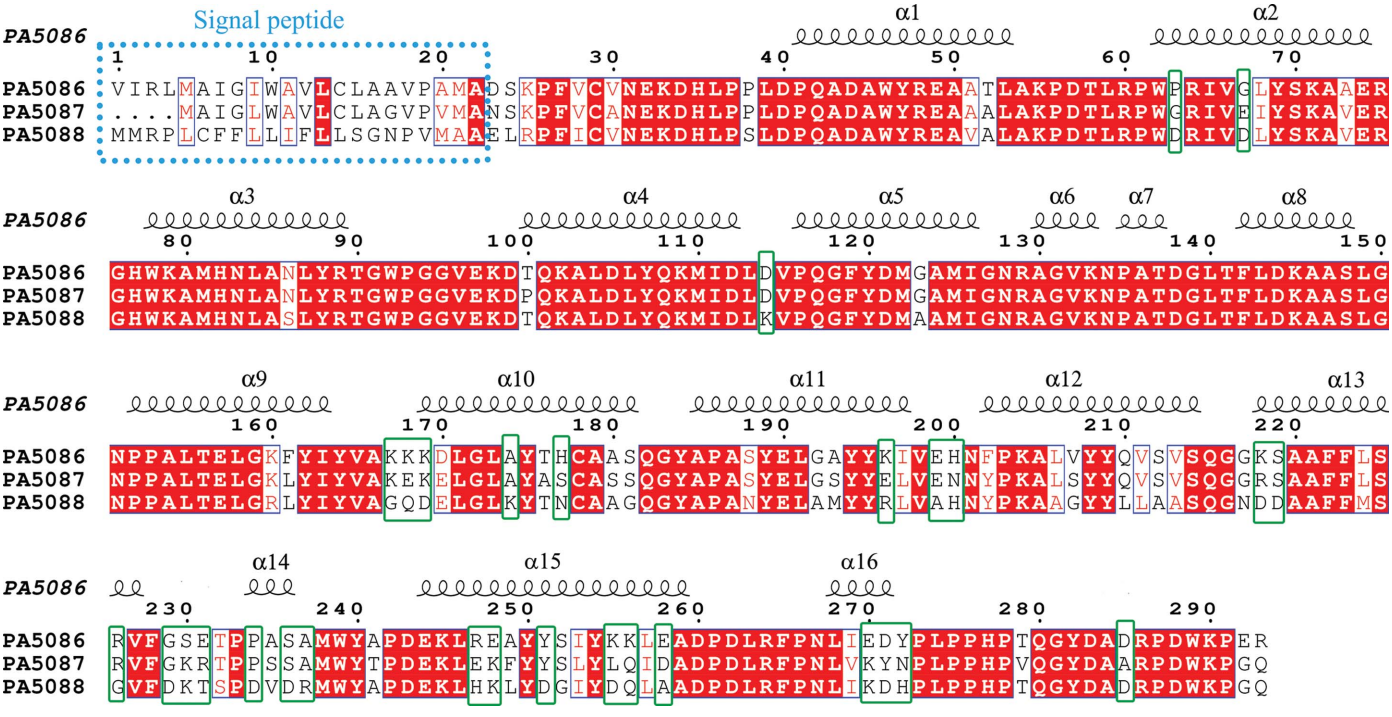

Figure 3
Sequence alignment of PA5086, PA5087 and PA5088. The α-helices in PA5086 are labeled. The different distributions of basic and acidic residues among the proteins are marked by green rectangles.

the search model in *phenix.phaser* (Liebschner *et al.*, 2019) and structure determination was performed by *phenix.autobuild* (Liebschner *et al.*, 2019).

2.4. Structure solution and refinement

The initial model was manually built and adjusted with *Coot* (Emsley *et al.*, 2010) and further refined using *phenix.refine* (Liebschner *et al.*, 2019). The quality of the final model was checked with *MolProbity* (Chen *et al.*, 2010). Data-collection and refinement statistics are given in Tables 3 and 4, respectively.

PyMOL (version 1.2; Schrödinger) was used to prepare structural figures. Sequence alignment was performed by *ClustalOmega* (Sievers *et al.*, 2011). The figure showing the sequence alignment was generated by *ESPript* (Robert & Gouet, 2014). Electrostatic potentials were calculated using the *PDB2PQR* server with the AMBER force field and were rendered using *PyMOL* in conjunction with the *APBS* plugin (Dolinsky *et al.*, 2004; Baker *et al.*, 2001).

3. Results and discussion

PA5086 is composed of 16 α-helices that can be further categorized into six consecutive SLRs. The overall structure of PA5086 is shown in Fig. 1. In contrast to the previously reported structures of canonical SLRs, in which the intra-repeat and inter-repeat angles between adjacent helices are always well conserved and the SLRs are always 36 amino-acid residues long (Grant & Greenwald, 1996; Lüthy *et al.*, 2004; Urosev *et al.*, 2013), the six SLRs in PA5086 are distinct in length and conformation, thus folding into a super-ring form rather than the canonical super-helical form (Grant & Greenwald, 1996; Lüthy *et al.*, 2004; Urosev *et al.*, 2013). Similar to the structural features of PA5088 and PA5087, the super-ring fold of PA5086 is stabilized by an ionic bond between Lys55 and Asp262 (Yang *et al.*, 2016).

The sequence identity between PA5086 and PA5087 is 85% and that between PA5086 and PA5088 is 73%. With such high sequence identities, structure alignments gave a root-mean-square deviation (r.m.s.d.) of 0.87 Å (260 aligned C^{α} atoms) between PA5086 and PA5087 (PDB entry 5jkp; Yang *et al.*, 2016) and an r.m.s.d. of 1.80 Å (252 aligned C^{α} atoms) between PA5086 and PA5088 (PDB entry 5jjo; Yang *et al.*, 2016).

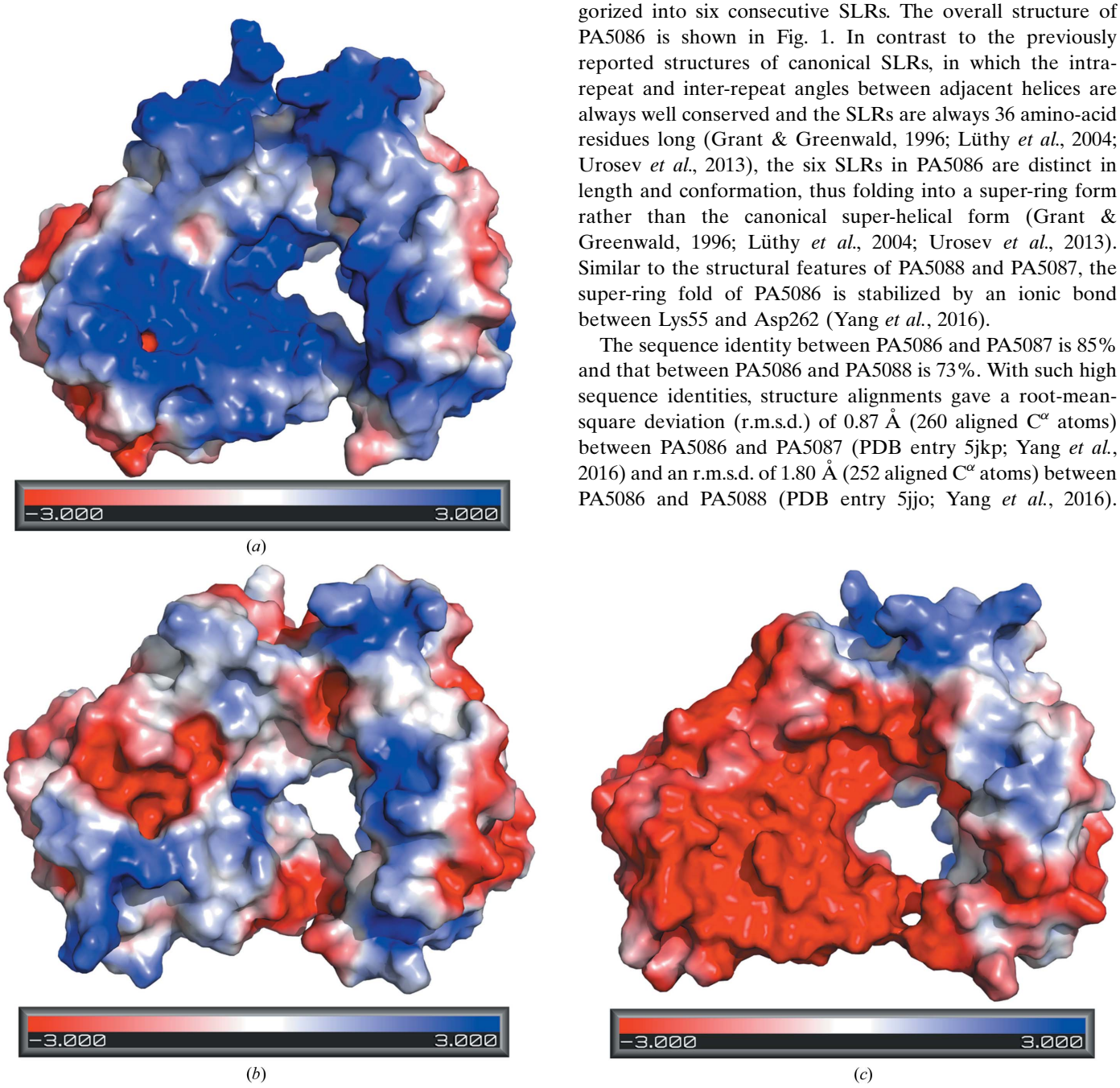

Figure 4
Electrostatic potential surfaces of PA5086 (*a*), PA5087 (*b*) and PA5088 (*c*).

Structure and sequence alignments among the three PldB immunity proteins are shown in Figs. 2 and 3, respectively.

The sequence identities among the first nine α-helices of these three proteins, which mainly include the first three SLRs, are quite high, whereas the larger differences among residues are concentrated in their SLR4 and SLR6 units (Fig. 3). These residue differences do not greatly affect the overall structures, but result in large divergences in the electrostatic potential surfaces among the structures.

The theoretical pI values of PA5086, PA5087 and PA5088 are 6.67, 7.11 and 5.49, respectively. The electrostatic potential surface of PA5086 from the viewpoint of Fig. 1 (top) is largely electropositive (Fig. 4*a*), whereas the electrostatic potential for the same surface area of PA5088 is predominantly negative (Fig. 4*c*). In the case of PA5087, the same electrostatic potential surface area possesses both electropositive and electronegative patches (Fig. 4*b*). The divergences in the electrostatic surfaces are mainly caused by differences in the distributions of basic and acidic residues (Fig. 3), especially for residues in SLR4, SLR5 and SLR6.

The solvent-accessible surface areas of the PA5086, PA5087 and PA5088 structures are 13 491, 13 671 and 13 627 Å^2, respectively. The structure formed by canonical SLRs usually creates an amphipathic groove that functions as a scaffold for protein–protein interactions, and this groove might be suitable for the recognition of target proteins (Das *et al.*, 1998). In the case of PA5086, PA5087 and PA5088 a hole is formed in the center of each super-ring fold, with different electrostatic potentials for passage through each hole (Fig. 4), which might play an important role in the interactions with toxins.

PldA and PldB are two trans-kingdom effectors that can affect both prokaryotic and eukaryotic cells (Jiang *et al.*, 2014). Although they are both categorized into the same Tle5 protein family, their cognate immunity proteins show great structural divergence. PA3488, the cognate immunity protein of PldA, adopts a crab claw-shaped structure (Yang *et al.*, 2017), whereas PA5086, PA5087 and PA5088 have super-ring folds formed by six SLR units. This suggests that the structures of PldA and PldB may also have major differences.

PA5086, PA5087 and PA5088 function equally well in suppressing PldB toxicity and they combine to contribute to inhibition of PldB in a dose-dependent manner (Jiang *et al.*, 2014). In our previous study, we performed molecular-docking experiments using the structures of PA5088 and PA5087 against the structure of *Streptomyces* PLD (PDB entry 2ze4; A. Suzuki, K. Kakuno, R. Saito, Y. Iwasaki, T. Yamane & T. Yamane, unpublished work). We proposed two toxin–antitoxin interaction models via aromatic stacking by the conserved aromatic residues Tyr189, Tyr209, Phe222, Phe223 and Tyr254 on SLR5 and SLR6, or Tyr282 and Trp289 on the C-terminal tails of PA5088 and PA5087 (Yang *et al.*, 2016). We found that these aromatic residues were also conserved in PA5086 in both the sequence and structure, and therefore they might provide similar PldB-binding affinities.

It is interesting to consider why PldB requires three immunity proteins instead of one as found in most other T6SS effectors. One theory suggests that the 'stockpiling' of similar immunity proteins may protect bacteria against similar effectors from different species (Jiang *et al.*, 2014). Our findings have greatly supported this theory by showing the vast divergences in the electrostatic potential surfaces of similar immunity proteins. PA5086, PA5087 and PA5088 may have different affinities for different PLD effectors from different species owing to their distinct surface potentials, and thus they should provide *P. aeruginosa* with better protection in competition with bacterial rivals.

Acknowledgements

We are grateful to the staff members at BSRF for sample testing and data collection.

Funding information

Funding for this research was provided by: National Natural Science Foundation of China (grant No. 31700651); National Basic Research Program of China (973 Program) (grant No. 2017YFA0504900) and Beijing Municipal Science and Technology Commission (grant No. Z191100007219007).

References

Baker, N. A., Sept, D., Joseph, S., Holst, M. J. & McCammon, J. A. (2001). *Proc. Natl Acad. Sci. USA*, **98**, 10037–10041.
Chen, V. B., Arendall, W. B., Headd, J. J., Keedy, D. A., Immormino, R. M., Kapral, G. J., Murray, L. W., Richardson, J. S. & Richardson, D. C. (2010). *Acta Cryst.* D**66**, 12–21.
Das, A. K., Cohen, P. W. & Barford, D. (1998). *EMBO J.* **17**, 1192–1199.
Dolinsky, T. J., Nielsen, J. E., McCammon, J. A. & Baker, N. A. (2004). *Nucleic Acids Res.* **32**, W665–W667.
Emsley, P., Lohkamp, B., Scott, W. G. & Cowtan, K. (2010). *Acta Cryst.* D**66**, 486–501.
Grant, B. & Greenwald, I. (1996). *Genetics*, **143**, 237–247.
Ho, B. T., Dong, T. G. & Mekalanos, J. J. (2014). *Cell Host Microbe*, **15**, 9–21.
Hood, R. D., Singh, P., Hsu, F., Güvener, T., Carl, M. A., Trinidad, R. R., Silverman, J. M., Ohlson, B. B., Hicks, K. G., Plemel, R. L., Li, M., Schwarz, S., Wang, W. Y., Merz, A. J., Goodlett, D. R. & Mougous, J. D. (2010). *Cell Host Microbe*, **7**, 25–37.
Jiang, F., Waterfield, N. R., Yang, J., Yang, G. & Jin, Q. (2014). *Cell Host Microbe*, **15**, 600–610.
Kabsch, W. (2010). *Acta Cryst.* D**66**, 125–132.
Liebschner, D., Afonine, P. V., Baker, M. L., Bunkóczi, G., Chen, V. B., Croll, T. I., Hintze, B., Hung, L.-W., Jain, S., McCoy, A. J., Moriarty, N. W., Oeffner, R. D., Poon, B. K., Prisant, M. G., Read, R. J., Richardson, J. S., Richardson, D. C., Sammito, M. D., Sobolev, O. V., Stockwell, D. H., Terwilliger, T. C., Urzhumtsev, A. G., Videau, L. L., Williams, C. J. & Adams, P. D. (2019). *Acta Cryst.* D**75**, 861–877.
Lüthy, L., Grütter, M. G. & Mittl, P. R. (2004). *J. Mol. Biol.* **340**, 829–841.
Potterton, L., Agirre, J., Ballard, C., Cowtan, K., Dodson, E., Evans, P. R., Jenkins, H. T., Keegan, R., Krissinel, E., Stevenson, K., Lebedev, A., McNicholas, S. J., Nicholls, R. A., Noble, M., Pannu, N. S., Roth, C., Sheldrick, G., Skubak, P., Turkenburg, J., Uski, V., von Delft, F., Waterman, D., Wilson, K., Winn, M. & Wojdyr, M. (2018). *Acta Cryst.* D**74**, 68–84.
Robert, X. & Gouet, P. (2014). *Nucleic Acids Res.* **42**, W320–W324.
Russell, A. B., Hood, R. D., Bui, N. K., LeRoux, M., Vollmer, W. & Mougous, J. D. (2011). *Nature*, **475**, 343–347.

Russell, A. B., LeRoux, M., Hathazi, K., Agnello, D. M., Ishikawa, T., Wiggins, P. A., Wai, S. N. & Mougous, J. D. (2013). *Nature*, **496**, 508–512.
Sievers, F., Wilm, A., Dineen, D., Gibson, T. J., Karplus, K., Li, W., Lopez, R., McWilliam, H., Remmert, M., Söding, J., Thompson, J. D. & Higgins, D. G. (2011). *Mol. Syst. Biol.* **7**, 539.
Urosev, D., Ferrer-Navarro, M., Pastorello, I., Cartocci, E., Costenaro, L., Zhulenkovs, D., Maréchal, J. D., Leonchiks, A., Reverter, D., Serino, L., Soriani, M. & Daura, X. (2013). *BMC Struct. Biol.* **13**, 19.
Winn, M. D., Ballard, C. C., Cowtan, K. D., Dodson, E. J., Emsley, P., Evans, P. R., Keegan, R. M., Krissinel, E. B., Leslie, A. G. W., McCoy, A., McNicholas, S. J., Murshudov, G. N., Pannu, N. S., Potterton, E. A., Powell, H. R., Read, R. J., Vagin, A. & Wilson, K. S. (2011). *Acta Cryst.* D**67**, 235–242.
Yang, X.-Y., Li, Z.-Q., Gao, Z.-Q., Wang, W.-J., Geng, Z., Xu, J.-H., She, Z. & Dong, Y.-H. (2017). *Protein Sci.* **26**, 2083–2091.
Yang, X.-Y., Li, Z.-Q., She, Z., Geng, Z., Xu, J.-H., Gao, Z.-Q. & Dong, Y.-H. (2016). *FEBS Lett.* **590**, 2787–2796.